

Catalysis

Divergent Carbocatalytic Routes in Oxidative Coupling of Benzofused Heteroaryl Dimers: A Mechanistic Update

David S. Casadio⁺,^[a] Santeri Aikonen⁺,^[a] Anna Lenarda,^[a] Martin Nieger,^[a] Tao Hu,^[b] Stefan Taubert,^[a] Dage Sundholm,^[a] Mikko Muuronen,^[a] Tom Wirtanen,^[a] and Juho Helaja^{*[a]}

Abstract: Mildly thermal air or HNO₃ oxidized activated carbons catalyse oxidative dehydrogenative couplings of benzo[b]fused heteroaryl 2,2'-dimers, e.g., 2-(benzofuran-2-yl)-1*H*-indole, to chiral 3,3'-coupled cyclooctatetraenes or carbazole-type migrative products under O₂ atmosphere. DFT cal-

culations show that the radical cation and the Scholl-type arenium cation mechanisms lead to different products with 2-(benzofuran-2-yl)-1*H*-indole, being in accord with experimental product distributions.

Introduction

Carbocatalytic conversions cover a wide range of acid catalysed reactions and oxidative transformations. For example, acidic or redox centres embedded in the carbon matrix are known to catalyse reactions such as substitutions, additions, (de)hydrations, (de)hydrogenations, and couplings of organic aryl substrates.^[1] In many reported carbocatalysed C–C bond forming reactions the net reaction, i.e., oxidative dehydrogenative (ODH) conversion, has been reported to proceed via acid catalysed, Friedel–Crafts (FC) type mechanism.^[2] Furthermore, we^[3a,b] and others^[4] have demonstrated that carbocatalytic aryl–aryl couplings can proceed through a SET-based process as well.^[3a] We concluded in our recent experimental–computational study that in carbocatalysis both mechanisms can operate depending on the substrate and used catalyst.^[3b] The reaction mechanisms, however, cannot always be easily distinguished. Abundantly, this has been shown by diverse transition metal (TM), molecular quinone, and other oxidant, mediated ODH-aryl couplings, which are known to proceed either

through arenium cation (ac)^[5] (Scholl reaction) or radical cation (rc)^[6] pathways.^[7]

Our research group has recently been developing new carbocatalytic synthetic methods for ODH aryl–aryl couplings that can be utilised instead of TM mediated analogues. Importantly, the difficultly accessible cycloocta-1,3,5,7-tetraenes (COTs) recently captured our interest when we managed to catalyse the synthesis of tetraindole COT via Au/C catalytic cascade reaction from 1,4-bis-(*o*-aniline)butadiyne (Figure 1c).^[3c]

[a] D. S. Casadio,⁺ Dr. S. Aikonen,⁺ Dr. A. Lenarda, Dr. M. Nieger, Dr. S. Taubert, Prof. D. Sundholm, Dr. M. Muuronen, Dr. T. Wirtanen, Dr. J. Helaja
Department of Chemistry, University of Helsinki
A. I. Virtasen aukio 1, P.O. Box 55, 00014 Helsinki (Finland)
E-mail: juho.helaja@helsinki.fi

[b] Dr. T. Hu
Research Unit of Sustainable Chemistry, Faculty of Technology
University of Oulu, 90014 Oulu (Finland)

[†] These authors contributed equally to this work.

Supporting information and the ORCID identification number(s) for the author(s) of this article can be found under:
<https://doi.org/10.1002/chem.202005433>.

© 2021 The Authors. Chemistry - A European Journal published by Wiley-VCH GmbH. This is an open access article under the terms of the Creative Commons Attribution Non-Commercial NoDerivs License, which permits use and distribution in any medium, provided the original work is properly cited, the use is non-commercial and no modifications or adaptations are made.

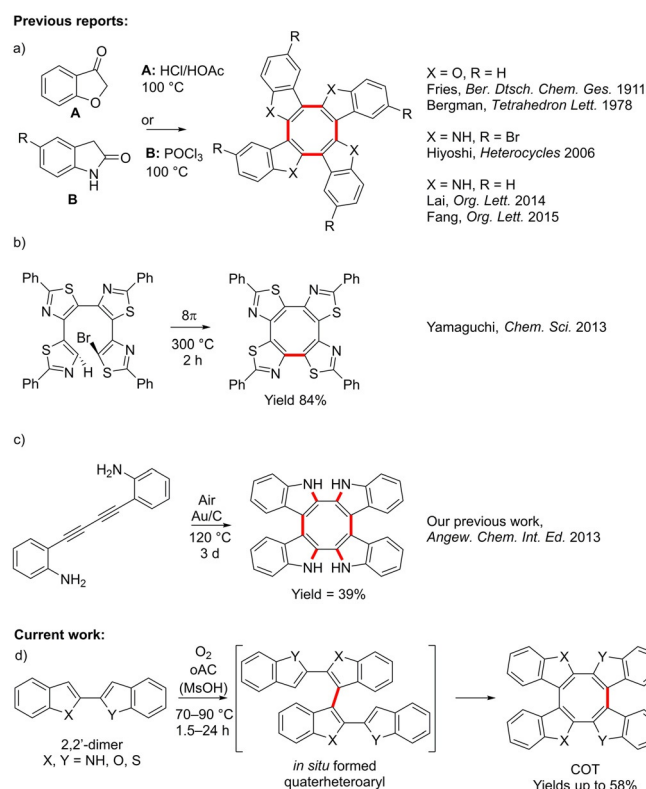


Figure 1. Selected one-pot accesses to heteroaryl fused COTs.

Differently substituted COTs have been synthesised via different TM mediated reactions,^[8–10] but, nevertheless, the protocols for heteroarene based COT synthesis remain scarce. This is surprising since COTs have unique molecular properties,^[11,12] are present in natural products,^[13] and have potential use in future material chemistry applications.^[14] Inspiringly, Fries and Pfaffendorf reported a one-pot tetramerization protocol of 3(2*H*)-benzofuranone to tetrabenzofuran COT (Figure 1 a),^[15a] for which the structure was later verified by Bergman and Egestad.^[15b] Analogously, Hiyoshi and co-workers discovered a one-pot metal-free tetramerization of 5-bromoindolin-2-one to C_{2v} -symmetric tetraindoles with $POCl_3$ in chlorobenzene,^[16a] while equivalent methodology in neat $POCl_3$ afforded unsubstituted analogues (Figure 1 a).^[16b,c] Both tetraindoles were received in modest yields (5.5%–16%). For a comparison, Yamaguchi and co-workers developed a high-yielding (72–84%) thermal 8π -electrocyclic protocol for thiazole fused COTs.^[17] In this reaction, a terminal Br leaving group and high temperatures ($\geq 260^\circ\text{C}$) were necessary to trigger the COT-cyclization (Figure 1 b). The drawback of this method is the laborious synthesis of the mono-halogenated quaterheteroaryl substrates that requires eight steps with an overall yield of 16% in the case of quaterheteroaryl in Figure 1 b.^[17]

We have previously demonstrated that oxidised activated carbon (oAC) can be utilised as a catalyst in the ODH C–C homocoupling reaction of different (hetero)aryls.^[3] The aryl–aryl ODH C–C-couplings^[7] are generally considered to operate via reaction mechanism involving an $rc^{[6]}$ or an $ac^{[5]}$ as the key intermediate. We previously concluded^[3b] that both the mechanisms are energetically close to each other and, therefore, can co-exist. As a result, the operative mechanism strongly depends on the redox potential and the proton affinity of the quinoidic catalyst and the substrate. Thus, we reasoned that we could utilise oxidative carbocatalysis and build the quaterheteroaryl derivatives in situ from the 2,2'-dimers (Figure 1 d) and cyclize them to the corresponding COTs. As a research premise, we chose to first investigate the plausible reaction mechanisms and use the information to guide us in the reaction development. Herein, we report the mechanism-based method development for the synthesis of different COT tetraheteroaryls and the effect of different mechanisms to the reaction outcome.

Results and Discussion

Electrocyclization and dearomatization

First, we inspected the computational activation free energy for the 8π -electrocyclization of the quaterheteroaryl dimer **2a** derived from the 2-(benzofuran-2-yl)-1*H*-indole monomer **1a**. We chose **1a** as the model compound because it can be readily prepared by a two-steps synthesis (SI). Unfortunately, the activation free energy barrier for the neutral Möbius aromatic C–C bond formation step **TS3** was too high in energy for the reaction to be conducted at typical temperatures used for organic synthesis: $36.7\text{ kcal mol}^{-1}$ (Figure 2 and Supporting Information). This is in line with what was previously reported for thia-

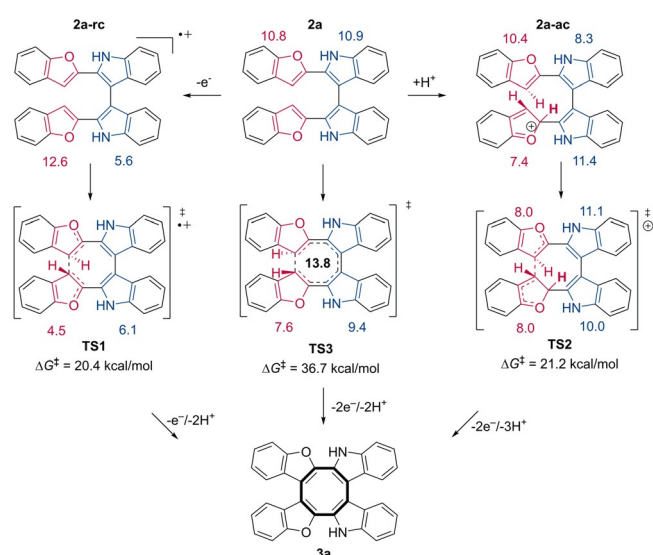


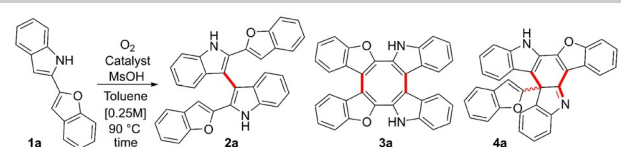
Figure 2. Different mechanisms for C–C bond formation in quaterheteroaryl **2a** and the activation free energies. Left: rc C–C bond formation, centre: 8π electrocyclization, and right: ac C–C bond formation. Ring current susceptibilities in nA/T. See Supporting Information for further details.

zoles by Yamaguchi.^[17] In addition, Yamaguchi and co-workers have demonstrated that oxidation of one or more of the thiophene rings in thiophene-fused bisdehydro[12]annulene to thiophene-*S,S*-dioxides dearomatizes the heteroaryl and promotes the 8π electrocyclization.^[18] Since the reaction conditions of our carbocatalysis are both oxidising and acidic,^[3] we inspected whether one-electron oxidation or protonation of the quaterheteroaryl could achieve similar dearomatization effect and accelerate the reaction rate (Figure 2).

Indeed, one-electron oxidation (**2a-rc**, Figure 2) reduced the ring-current strength in the pyrrole subrings from 10.9 to 5.6 nA/T while the protonation of one of the furan-rings (**2a-ac**) lowered the ring-current strength in the furan-ring and one pyrrole-ring from 10.8 to 7.4 nA/T and from 10.9 to 8.3 nA/T, respectively. Subsequently, the activation free energy barriers for the C–C bond formations were lowered by 16.3 and 15.5 kcal mol⁻¹ compared to **TS3** for **TS1** and **TS2**, respectively. This led us to the conclusion that it is possible to improve the previous carbocatalytic methodology for COT synthesis^[3c] with oAC and molecular acid additives since our recent studies have indicated that acid additives increase the oxidative power of quinones^[5,19] and protonate the substrate.^[3b] This could lead to a significant broadening of the substrate scope and new COT substrates.

Catalyst screening

We started our study by screening several carbon materials for the desired ODH catalysis, using **1a** as the model substrate and the reaction conditions we previously applied for oAC catalysed homocouplings of benzo-fused heterocycles:^[3a] 224 mg of oAC per 1 mmol of SM under O_2 atmosphere in toluene at 90°C (Table 1). We tested first HNO_3 oxidized AC (oAC- HNO_3)^[3a] and isolated the homocoupling product **2a** exclusively in a

Table 1. Screening of carbocatalysts and molecular quinones.


Entry	Catalyst/reagent (equiv) ^[a]	MsOH (equiv)	t (h)	Yield ^[b] (%) 2 a:3 a:4 a
1	oAC-HNO ₃ (1)	0	24	80:0:0
2	oAC-HNO ₃ (3)	3	5	0:0:79
3	oAC-air(Δ) (1)	0	24	75:0:0
4	oAC-air(Δ) (5)	5	1.3	0:58:0
5	oAC-air(Δ) (5) ^[c]	5	1.3	0:11:0
6	GO ^[d] (1)	1	4.5	0:0:16
7	oCNT ^[e] (5)	5	5	24:9:7
8	PQ (1) ^[f]	1	20	–
9	AQ (1)	1	24	2:0:0
10	DDQ (1)	0	1.5	–
11	FeCl ₃ (0.1)	0	23.5	53:0:0

[a] Catalyst equiv = 224 g mol⁻¹ (of SM). [b] Isolated yield after flash column chromatography. [c] Under Ar. [d] Few Layer modified Hummer's (Cheaptubes.com). [e] ref. [3b]. [f] Substrate reacted with PQ (S2 in Supporting Information).

high yield of 80% (entry 1). Promisingly, almost as high yield of **2a** (75%) was obtained with thermally air oxidized and under argon decarboxylated AC (oAC-air(Δ))^[20] (entry 3) under the same conditions. Surprisingly, when 3 equiv of methanesulfonic acid (MsOH) was used with oAC-HNO₃, a high 79% yield of an unexpected cyclized 6-ring dearomatized product **4a** with a migrated benzofuranyl group was received (entry 2). A variety of indole transformation methods based on dearomatization have been reported in the literature,^[21] but, however, the acid co-catalysed oxidative conversion involving aryl migration is thus far unreported and will be studied in detail elsewhere. Finally, after screening both oAC catalysts with various loadings of catalyst and MsOH while varying time (see Table S2, Supporting Information), the increase of both oAC-air(Δ) (5 equiv) and MsOH (5 equiv) delivered gratifyingly a 58% isolated yield of the desired COT-product **3a** (entry 4).

In addition, we studied several different carbon-based heterogeneous catalysts and homogeneous oxidants that we and others have found highly suitable for similar reactions (Table 1). A catalytic trial with graphene oxide (GO)^[3b] delivered only the migratory product **4a** in a 16% yield (entry 6). Characteristically, GO has a higher amount of carboxylic groups than carbonyl groups and it is often utilized as an acid catalyst in, e.g., FC type reactions.^[2,22]

Recently, we have demonstrated that HNO₃-oxidized carbon nanotubes (oCNTs) can successfully catalyse various intra- and intermolecular ODH couplings.^[3b] However, for substrate **1a**, oCNT with MsOH additive delivered a mixture of **2a**, **3a**, and **4a**, with 24%, 9%, and 7% yields, respectively.

Previously, molecular quinones such as 2,3-dichloro-5,6-dicyano-1,4-benzoquinone (DDQ),^[23] 9,10-phenanthrene-quinone (PQ), and anthraquinone (AQ), have been used to mimic the C=O/(carbonyl/quinone) active site of carbocatalysts.^[3b,24] In our hands, AQ with 1 equiv of MsOH gave the highest yield

(2%) of monocoupled product **2a** (Table 1, entry 9). Meanwhile, PQ coupled with **1a**'s indole C3-position (Table 1, entry 8) yielding a dehydrated product, 10-(2-(benzofuran-2-yl)-1*H*-indol-3-yl)phenanthren-9-ol (S2, Supporting Information). Similar couplings between indoles and quinones have been previously reported with Lewis-acid catalysis at elevated temperatures or by photochemical reactions (SI).^[25] Surprisingly, DDQ decomposed **1a** completely in 1.5 h (entry 10).

In addition to DDQ,^[21] iron(III) chloride (FeCl₃) is known to catalyse both Scholl-type couplings,^[7] and indole homocouplings under oxygen atmosphere.^[26] Here, however, FeCl₃ (0.1 equiv) monocoupled **1a** to **2a** with a 53% yield, but failed to give any COT or migration product (entry 11 in Table 1).

Since molecular quinones in acidic conditions (entries 8 and 9, Table 1) failed to promote the formation of products **3a** and **4a**, we hypothesised that the carbon surface helps to stabilise the different reactive species during catalysis. Thus, we added non-oxidized, demetallized AC (2 equiv = 448 g mol⁻¹ (of SM)) to the reaction mixture with PQ (1 equiv) and MsOH (1 equiv) and after running reaction for 24 h at 90 °C under air we received **3a** and **4a** in 32% and 3% yields, respectively (Figure 3). Lowering the AC loading to 1 equiv (224 g mol⁻¹ (of SM)) produced higher conversion but also higher decomposition of SM (96% conversion but overall 30% yield), with **3a** and **4a** in 20% and 10% yield, respectively. The use of a 0.5 equiv (112 g mol⁻¹ (of SM)) loading of AC delivered no **3a** and 4% of **4a** with modest 35% conversion of SM. Interestingly, with 1 equiv loading of AC and MsOH and replacing PQ with AQ delivered **4a** and **3a** in 16% and 13% yield, respectively. Control reactions demonstrated that AC, PQ, and AC supported PQ did not catalyse the reaction, while MsOH with AC (224 g mol⁻¹ (of SM)) was able to deliver some conversion of **2a** to **3a** and **4a**, 12% and 8%, respectively. This background reaction took place probably due to some residual oxygen containing functional groups in AC.^[20] Nevertheless, it seems that unmodified AC has a beneficial effect for the reactions carried out with molecular quinones by stabilization of substrates, intermediates, or products. This may arise either from functional groups in the carbon material or π -stacking interactions of the graphitic surface with the reactive species.^[27]

Overall, the optimization of reaction conditions shows that the developed oAC-catalysts are far superior for coupling of

Reactions run over 24 h at 90 °C in toluene under air:

		AC (1) or PQ	PQ MsOH	decomposition /polymerization
no reaction		←	→	→
		or AC(1) + PQ		
			MsOH	2a + 3a + 4a
			AC (1)	27% 12% 8%
			PQ	AC(x) 2a + 3a + 4a
			MsOH	0.5 65% 0% 4%
2a + 3a + 4a		AQ	AC (1)	1.0 4% 20% 10%
20% 13% 16%		MsOH	AC(x equiv)	2.0 14% 32% 3%

Figure 3. Control tests to explore the stoichiometric quinoidic reactivity of **2a** in presence of AC (1 equiv = 224 g mol⁻¹ (of SM)), PQ or AQ (1 equiv) and MsOH (1 equiv) performed under air.

highly sensitive benzofused heteroarenes in comparison to the other tested catalysts and oxidants, such as FeCl_3 and DDQ. The X-ray photoelectron spectroscopy (XPS) analysis of the recovered carbon material indicated that quinoidic content was retained during the reaction and thus supports the catalytic nature of the oACs (see Table S4, Figure S4). Additionally, under argon atmosphere only 11% of **3a** could be obtained (entry 5) in otherwise standard reaction conditions. Intriguingly, the course of reaction is so delicate that different distributions of COT and migration products were obtained by combinations of oAC-air(Δ) and oAC- HNO_3 with the acid additives.

Interestingly, Nakayama and co-workers^[28] have recently demonstrated how intramolecular hydrogen bonding (HB) in anthraquinone derivatives effectively inhibits intermolecular HB between the carbonyl and HB donors. The striking difference between the oAC-air(Δ) and oAC- HNO_3 is that the latter has acidic HB donors abundantly present in the material that can disfavour intermolecular HB and make the protonation of the substrate more favourable. On the other hand, in oAC-air(Δ), the acidic HB donors are removed from the material by heat-treatment.^[20] this subsequently can favour HB between the carbonyl groups of the material and MsOH and disfavour protonation of the substrate.

Computed reaction mechanisms

To understand the effect of the catalyst on the product selectivity, i.e., how oAC-air(Δ) catalyses the transformation from **1a** to **3a** (entry 4 in Table 1) while oAC- HNO_3 catalyses the transformation from **1a** to **4a** (entry 2 in Table 1), we investigated computationally how both products are formed via the rc and ac reaction mechanisms at DFT level in toluene. We recently found^[3b] that *ortho*-benzoquinone (o-BQ) and AQ serve as good model structures for carbocatalysts with different redox potentials and proton affinities and were, therefore, used for further investigations. The control reactions with PQ and AQ (see Table 1 and Figure 3) demonstrated that molecular quinones can be used as models for the oACs.

The model quinones are protonated in intermediate **A** (Figure 4), which facilitates the comparison of proton affinities between the quinonium cation and heteroarene system. Also, the acid additive promotes the oxidative power of the quinones.^[6] The absolute protonation energetics, however, highly depend on the stability of the conjugate base, while at the same time the anion stabilization effects of the carbon material are difficult to model. Thus, protonated quinonium cations are used instead of explicit MsOH. Mechanisms with higher activation free energies, for example, the rc 6-ring formation, are presented in Supporting Information.

The computed activation free energies for both pathways are shown in Figure 4. **TS1** is the selectivity determining transition state for rc mechanism and **TS2** correspondingly for the ac mechanism. These routes compete and thus the operating mechanism should be the one with a lower activation free energy, **TS1** or **TS2**. The o-BQ model catalyst is capable of oxidizing substrate **2a** exergonically driving the selectivity towards 8-ring product **3a** while the other pathway is not ener-

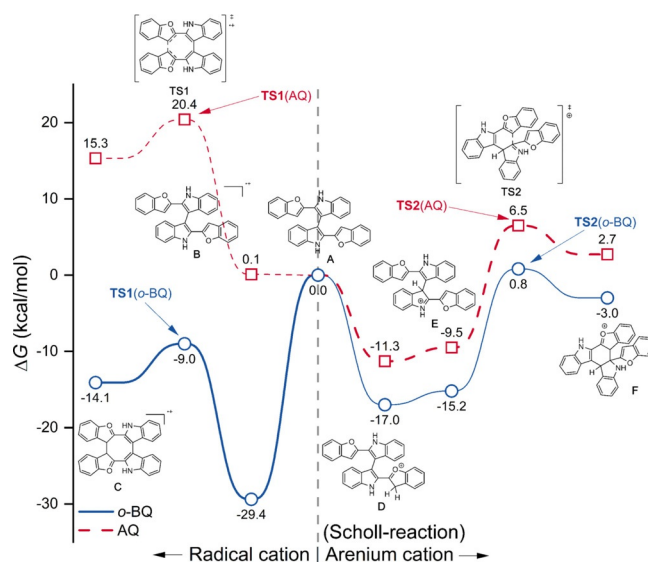


Figure 4. Gibbs free energy profiles for rc 8-ring formation (to left) and ac 6-ring formation (to right) for **2a**. Free energies are balanced with o-BQ (solid blue lines with squares) and AQ (dashed red lines with circles). Thick line is favoured and thin line disfavoured mechanism. All free energies are based on PW6B95-D3/def2-TZVPD//PBE0-D3/def2-TZVP level.

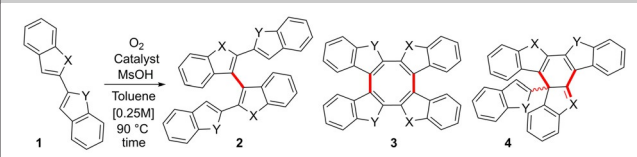
getically as feasible. The AQ catalyst, however, protonates the substrate exergonically and drives the selectivity towards the 6-ring product **4a**. The model thus explains how oAC-air(Δ) and oAC- HNO_3 catalysts can yield different products, as the electron affinity and proton affinity of the quinoidic catalyst determines the operative mechanism and the observed product selectivity.

Substrate scope

Next, we screened couplings of other benzofused heteroaryl dimers with oAC catalysts (Table 2). With 2,2'-biindole **1b**, the COT **3b** was isolated after 24 h in a 42% yield with only 1 equiv of oAC-air(Δ) as catalyst (entry 1). Using MsOH as additive decomposed **1b**. Without an excess of acid additive, substrate **1c** exhibited similar selectivity than **1a**: 1 equiv oAC-air(Δ) and 0.5 equiv of MsOH delivered an 85% isolated yield of **2c** (entry 2). With 2 equiv of both oAC-air(Δ) and MsOH, a 41% yield of migration product **4c** was received (entry 4). In addition, a small amount of **3c** (2%) was received after 6 h when the loading ratio was changed to 5:2 (entry 3).

Beyond the indole derivatives, both 2,2'-bibenzofuran **1d** and 2,2'-bibenzothiophene **1f** have been monocoupled to the respective dimers **2d** in 35% (entry 6) and **2f** in 37% (entry 8) yields. With a high 5 equiv loading of 1:1 oAC- HNO_3 /MsOH mixture, **1d** was successfully cyclized to COT **3d** in a 22% yield (entry 5) whereas **1f** did not yield any cyclized products under the same conditions (entry 8). The 2,2'-benzo[*b*]furan-benzo[*b*]thiophene COT product **3e**, instead, was isolated in a 36% yield from **1e** (entry 7).

Table 2. Carbocatalysed coupling reactions of benzofused biheteroaryls.



Entry	1	X–Y	oAC-HNO ₃ /air(Δ)Cat (equiv.) ^[a]	MsOH (equiv)	T (°C)	t (h)	Yield ^[b] 2x–4x
1	1b	NH–NH	air(Δ) (1)	–	90	24	42% 3b
2	1c	NH–S	air(Δ) (1)	0.5	90	24	85% 2c
3	1c	NH–S	air(Δ) (5)	2	90	6	2% 3c
4	1c	NH–S	air(Δ) (2)	2	90	16	41% 4c
5	1d	O–O	air(Δ) (5)	5	90	24	35% 2d
6	1d	O–O	HNO ₃ (5)	5	70	17	22% 3d
7	1e	O–S	HNO ₃ (5)	5	90	17	36% 3e
8	1f	S–S	HNO ₃ (3)	3	90	24	37% 2f

[a] Catalyst equiv = 224 g mol⁻¹ (of SM). [b] Isolated yields after flash column chromatography.

COTs' properties

In principle, the highly sterically strained COTs can exhibit enantiomerism with combination of *R,R*; *S,S*; *R,S* stereocentres. For **3a**, we resolved the enantiomers, measured electronic circular dichroism and computed the spectrum for the *R_oR_a* enantiomer (Figure 5), see Supporting Information for details. Additionally, the single crystal structure of **3d** shows the distorted tube-conformation of the COT (*R*,R**-enantiomer, Figure 5).

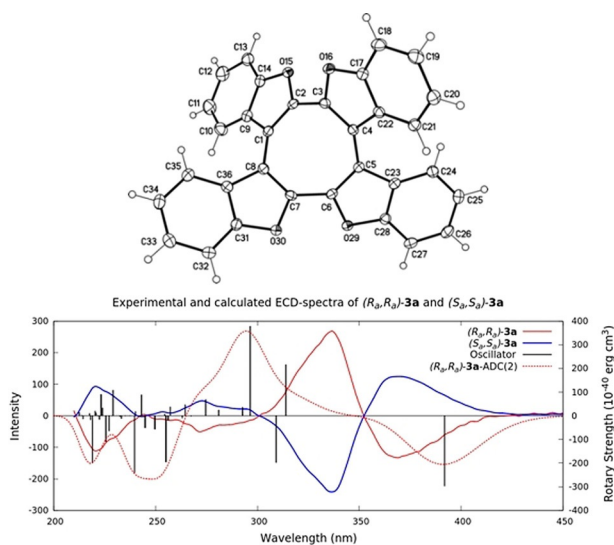


Figure 5. Above: X-ray crystal structure of tetrabenzofuran COT (**3d**). Below: Experimental and computed (ADC(2)/def2-TZVPPD) electronic circular dichroism spectra of **3a** enantiomers.

The cyclic voltammetry experiment in Figure 6 revealed two consecutive reversible one-electron oxidations at 0.14 and 0.37 V (vs. Fc/Fc⁺) for COT **3a**. In the dicationic state of **3a** the central COT ring is aromatic (see SI), as has been also reported in literature for other COT-structures.^[29]

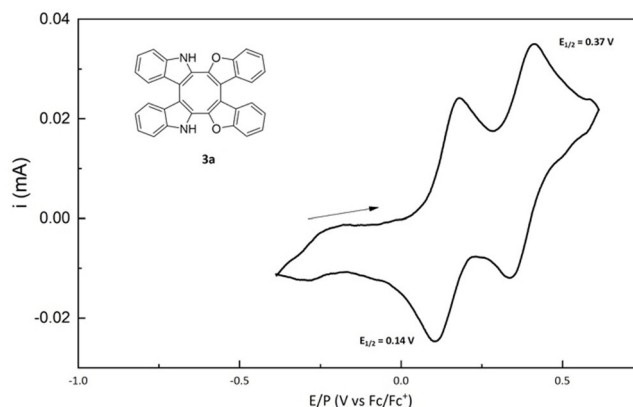


Figure 6. CV obtained on GCE in a 0.10 M NBu₄PF₆ solution in acetonitrile under Ar. Scan rate: 0.5 V s⁻¹.

Conclusions

In summary, C=O rich oAC materials (oAC-HNO₃ and oAC-air(Δ)) were prepared and a carbocatalytic cascade method was devised to synthesize sterically distorted benzofused heteroaryl cyclooctatetraenes or 6-ring cyclized partially dearomatized migration product from couplings of benzofused heteroaryl dimers. The starting materials can be prepared by established synthetic methods, and both the step-economy and overall yields were improved compared to other metal-free state-of-the-art synthesis of analogous COTs. The developed carbon materials exhibited enhanced catalytic performance compared to other carbon materials as well as to all tested homogeneous oxidants. Significantly, the different preparation methods of the catalytic carbon materials alter their surface properties and thus influence the reaction pathway. Our computational results rationalize the product selectivity of the two oAC based on the mechanism. The coexistence of the rc and ac (Scholl-reaction) mechanisms was confirmed as the former selectively yields the COT and the latter the migration product. We anticipate that the developed method can be applied to synthesis of other sensitive substrates as well and we are currently pursuing this in our laboratory. Particularly, role of the graphitic surface and residual functional groups in oxidative catalysis with oxidized carbon materials deserves more in-depth studies.

Experimental Section

Methods and materials

All reactions with AC were carried out in a Teflon capped vial equipped with a magnetic stirring bar under O₂ atmosphere. Reactions were monitored with thin layer chromatography (TLC) with SiO₂ on aluminium coated plates. Mixtures of EtOAc and *n*-hexane (from 1:4 to 1:1) were used as eluents. All oAC-catalysts were prepared from the same batch (Lot. H2430) of AC (100 mesh) obtained from Fluka. The catalytic activity of oACs was tested with the homocoupling reaction of 2-phenyl-indole as a standard (Table S1) to control the possible batch variability. NMR yields were measured with a Bruker 500 spectrometer using 1,3,5-trimethoxy-

benzene dissolved in [D₆]DMSO in a sealed capillary as an external standard. The crude products were dissolved in a measured amount of solvent and analysed with proton spectra. All the other NMR spectra were recorded on Varian 300, Bruker 400, and Bruker 500 spectrometers. High resolution mass spectra (EI⁺) were measured with MS JEOL JMS-700. Electrochemical tests were performed at room temperature using an Interface 1000 electrochemical workstation (Gamry Instruments). The set-up cell used for the experiments was a three-electrode system consisting of a platinum coil as the counter electrode, a Pt wire as pseudo-reference electrode with Fc/Fc⁺ as an internal standard and a glassy carbon electrode as a working electrode.

Computational details

Density functional theory (DFT) level computations were carried out with TURBOMOLE 7.3^[30] and ORCA 4.1^[31] program packages. TURBOMOLE was used for geometry optimisations, calculation of vibrational frequencies, and final single-point energies, whereas ORCA was used for transition state search. Lowest energy conformers and protomers were searched for using CREST^[32] and GFN-xTB.^[33] Structures were optimized with a dispersion corrected hybrid density functional, PBE0-D3,^[34,35] using def2-TZVP^[36] basis sets. Final single-point (sp) energies were calculated with PW6B95-D3^[37] hybrid functional utilizing diffuse triple-zeta basis sets, def2-TZVPD.^[38] The vibrational frequencies were computed on same level of theory as the geometries. The multipole accelerated resolution-of-identity approximation for the Coulomb term^[39] was used with TURBOMOLE with the corresponding auxiliary basis sets.^[40] The grid *m4* and default convergence criteria of 10⁻⁷ and 10⁻⁶ were used for density and energy, respectively. COSMO^[41] solvation model was used in all structure optimizations with dielectric constant of toluene (2.38), and for final energies using COSMO-RS solvation model in COSMOtherm19 program package^[42] with BP_TZVPD_FINE_19.ctd parameter file based on BP86^[43]/def2-TZVPD computational level. The Gibbs free energies in solution were calculated according to published protocol: $G = E_{\text{gas}}(\text{SCF}) + \text{c.p.} + G_{\text{solv}}$ ^[44] where $E_{\text{gas}}(\text{SCF})$ is the sp-energy in gas-phase at current level of theory, c.p. is the chemical potential calculated using the qRRHO approximation by Grimme,^[45] and G_{solv} is the solvation free energy of each species in toluene. All thermodynamic functions were calculated at 298.15 K and vibrational frequencies were used without scaling. The reference state for Gibbs free energies at room temperature is 1 bar of ideal gas and 1 mol of liquid solvent.^[44]

The electronic circular dichroism (ECD) spectrum of (*R_gR_g*)-**3a** was simulated at the ADC(2)^[46] level using the def2-TZVPPD^[36,38] basis sets on a geometry optimized at PW6B95-D3/def2-TZVP level in 2-propanol (17.9). We computed 40 vertical excitation using the reduced-virtual-space (RVS) approach with an energy threshold of 60 eV, which resulted in 846 frozen virtual orbitals in addition to the 36 frozen core orbitals.^[47,48] The CD spectrum was simulated by using the computed oscillator strengths as peak heights for the computed excitation energies, and by applying Gaussian broadening from following Equation (1).^[49,50]

$$f(E) = \frac{1}{\sigma\sqrt{\pi}} \sum_i E_i r_i \exp\left[-\left(\frac{E - E_i}{\sigma}\right)^2\right] \quad (1)$$

where E_i are the calculated excitation energies, R_i are the calculated oscillator rotary strengths, and a σ of 0.2 eV was used. The intensity of the experimental spectrum was scaled to same intensity as the simulated one.

The ring current susceptibilities (in nA/T) have been calculated using the GIMIC method^[51,52] for the optimized molecular structures. The ring currents have been calculated at the B3LYP^[53] level using the def2-TZVP basis set. For the closed shell molecules, the prerequisite NMR calculations were done using Turbomole 7.41^[30] and for the radicals, the prerequisite NMR calculations were done using Gaussian16.^[54] The ring currents were calculated at specific bonds by placing an integration plane across the bond halfway between the atoms. The integration plane goes from the midpoint of the ring and 10.0 bohr outside the ring. The integration plane is also extended 10.0 bohr below and above the ring. The magnetic field is directed perpendicularly to the bond and parallel to the plane. The spacing between the grid points in the integration plane was 0.02 a.u.

Preparation of thermally air oxidized AC, oAC-air^[20]

The AC was washed with dilute HCl to remove metal impurities. The carbon (16 g) and HCl (1 M, 128 mL) were loaded into a flask and the mixture was stirred at 70 °C for 17 h. The mixture was filtered thru (Whatman 5) filter paper in a Büchner funnel and washed with 3 L of deionized H₂O and dried in an oven at 140 °C for 16 h. The carbon material was then divided into four batches. Each individual batch (4 g) was placed into a ceramic crucible and heated in an oven under static air atmosphere for 16 h at 425 °C (14 °C min⁻¹ heating rate).

Thermal treatment of air oxidized AC, oAC-air(Δ)^[20]

The crucible with oAC-air carbon was cooled down to r.t. and then heated in a tubular oven under Ar atmosphere for 16 h at 450 °C (the used heating rate was 8 °C min⁻¹). The resulting oAC was then cooled down to r.t. and stored into a vial. Residual mass was 63–66%.

Preparation HNO₃ oxidized AC, oAC-HNO₃^[3a]

As above for the air oxidation, AC was washed in the same manner with dilute HCl to remove metallic impurities. Each 4 g batch was loaded into a glass flask and conc. (70%) HNO₃ was added dropwise until a slurry was formed (8 mL). After HNO₃ addition, the flask was attached with a tube to an empty Dreschel bottle from which tubing lead the formed gasses into a beaker filled with dilute NaOH (aq.). The flask was then heated at 140 °C for 16 h and afterwards kept under vacuum at 140 °C for 2 h. Product was then cooled down to r.t. Residual mass was 97%.

General procedure without additive (GP1)

Starting material and oAC catalyst (224 g mol⁻¹ of SM) were loaded into a vial and toluene was added to reach 0.25 M solution of substrate. Vial was sealed with a septa cap. Reaction container was degassed with three vacuum and refilling cycles from high vacuum line and O₂ balloon. After this the balloon was left attached on vial thru a needle. The reaction mixture was stirred at 90 °C for 1.5–24 h and cooled in a water bath to r.t. It was then filtered through Diatomaceous earth (Celite[®]) and the filter cake was washed with DCM. Solvents were evaporated and the crude products were purified by flash column chromatography using SiO₂ as stationary phase and mixtures of EtOAc:*n*-Hex as eluent.

General procedure with additive (GP2)

Catalysis was performed as GP 1 with 1–5 equiv MsOH as additive. After the reaction vial was cooled down to r.t. in water bath, and the reaction mixture was filtered through basic alumina and Celite and washed with DCM. Solvents were evaporated and the crude products were purified by a flash column chromatography using SiO₂ as a stationary phase and mixtures of EtOAc:*n*-Hex as eluent.

Synthesis and characterisation

Synthesis of 3a: Compound **3a** was prepared following the GP2 with **1a** (29.5 mg, 0.13 mmol), oAC-air(Δ) (140.1 mg) and MsOH (40.6 μ L, 0.62 mmol) with 1.3 h reaction time. Product was purified using flash column chromatography with silica as stationary phase and EtOAc:*n*-Hex (1:4) as eluent. Yield was 16.6 mg, 58%. ¹H NMR (500 MHz, [D₆]DMSO): δ = 11.95 (s, 2H), 7.75 (d, *J* = 8.9 Hz, 2H), 7.49–7.42 (m, 6H), 7.38–7.32 (m, 2H), 7.33 (d, *J* = 8.2 Hz, 2H), 7.23 (dd, *J* = 8.2, 7.0 Hz, 2H), 7.07 (dd, *J* = 8.1, 7.0 Hz, 2H). ¹³C NMR (75 MHz, DMSO): δ = 155.5, 146.9, 138.3, 127.0, 126.4, 125.6, 124.4, 123.6, 123.2, 121.0, 120.8, 119.6, 112.3, 112.1, 111.8, 111.8. HRMS calculated for [C₃₂H₁₈N₂O₂⁺]: 462.1368, found: 494.1377.

Synthesis of 3c: Compound **3c** was prepared following the GP2 with **1c** (62.7 mg, 0.25 mmol), oAC-air(Δ) (281.5 mg) and MsOH (32.6 μ L, 0.50 mmol) with 6 h reaction time. Product was purified using flash column chromatography with silica as fixed phase and EtOAc:*n*-Hex (1:4) as eluent. Yield was 1.4 mg, 2%. ¹H NMR (500 MHz, [D₆]DMSO): δ = 11.81 (s, 2H), 8.11 (d, *J* = 8.1 Hz, 2H), 7.44 (m, 4H), 7.38 (d, *J* = 8.0, 2H), 7.33 (dd, *J* = 8.2, 7.2, 2H), 7.20 (dd, *J* = 8.2, 7.0, 2H), 7.1 (d, *J* = 8.1, 2H), 7.05 (dd, *J* = 8.0, 7.0, 2H). ¹³C NMR (75 MHz, [D₆]DMSO): δ = 140.0, 138.0, 137.7, 134.3, 130.2, 128.4, 126.8, 125.1, 124.7, 124.4, 123.0, 122.8, 120.5, 119.6, 111.9, 110.9. HRMS calcd for [C₃₂H₁₈S₂O₂⁺]: 494.0911, found: 494.0899.

Synthesis of 3d: Compound **3d** was prepared following the GP2 at 70 °C with **1d** (44.5 mg, 0.19 mmol), oAC-HNO₃ (226.0 mg) and MsOH (61.7 μ L, 0.95 mmol) with 17 h reaction time. Product was purified using flash column chromatography with silica as stationary phase and EtOAc:*n*-Hex (1:40) as eluent. Yield was 9.8 mg, 22%. ¹H NMR (500 MHz, CDCl₃): δ = 7.63 (d, *J* = 8.4 Hz, 2H), 7.56 (d, *J* = 7.9 Hz, 2H), 7.43 (dd, *J* = 8.5, 7.2 Hz, 2H), 7.31 (t, *J* = 7.3 Hz, 2H). ¹³C NMR (126 MHz, CDCl₃): δ = 157.0, 143.4, 127.3, 126.4, 123.6, 122.1, 115.6, 112.2. HRMS calcd for [C₃₂H₁₆O₄⁺]: 464.1049, found: 464.1068.

Synthesis of 3e: Compound **3e** was prepared following the GP2 with **1e** (63.6 mg, 0.25 mmol), oAC-HNO₃ (286.0 mg) and MsOH (82.5 μ L, 1.3 mmol) with 24 h reaction time. Product was purified using flash column chromatography with silica as stationary phase and EtOAc:*n*-Hex (1:40) as eluent. Yield was 22.4 mg, 35%. ¹H NMR (500 MHz, CD₂Cl₂): δ = 7.94 (d, *J* = 8.2 Hz, 2H), 7.61 (d, *J* = 8.2 Hz, 2H), 7.59 (d, *J* = 7.7 Hz, 2H), 7.46–7.37 (m, 4H), 7.33–7.21 (m, 6H). ¹³C NMR (126 MHz, CD₂Cl₂): δ = 156.8, 148.0, 142.2, 138.9, 133.0, 131.9, 128.2, 126.3, 126.2, 125.4, 125.0, 123.9, 123.1, 122.1, 114.6, 112.3. HRMS calcd for [C₃₂H₁₆S₂O₂⁺]: 496.0592, found: 496.0578.

Synthesis of 4a: Compound **4a** was prepared following the GP2 with **1a** (11.9 mg, 51.0 μ mol), oAC-air(Δ) (33.1 mg) and MsOH (9.7 μ L, 0.15 mmol) with 5 h reaction time. Product was purified using flash column chromatography with silica as stationary phase and EtOAc:*n*-Hex (1:4 → 1:9) as eluent. Yield was 9.3 mg, 79%. ¹H NMR (500 MHz, [D₆]DMSO): δ = 12.67 (s, 1H), 8.41–8.36 (m, 1H), 8.26 (d, *J* = 8.2 Hz, 1H), 8.05–7.99 (m, 1H), 7.82–7.75 (m, 2H), 7.57–7.50 (m, 2H), 7.50–7.45 (m, 2H), 7.41 (td, *J* = 7.5, 1.1 Hz, 1H), 7.37 (dd, *J* = 7.7, 1.3 Hz, 1H), 7.33–7.28 (m, 2H), 7.28–7.23 (m, 1H), 7.11 (ddd, *J* = 8.4, 7.2, 1.5 Hz, 1H), 7.06 (td, *J* = 7.4, 1.1 Hz, 1H), 6.12 (d,

J = 0.9 Hz, 1H). ¹³C NMR (126 MHz, DMSO): δ = 175.9, 156.6, 156.5, 155.2, 154.2, 153.1, 137.6, 136.8, 129.4, 127.4, 126.2, 126.0, 125.9, 125.8, 125.1, 124.8, 124.3, 123.7, 123.6, 122.9, 121.3, 121.2, 121.1, 121.0, 120.3, 115.5, 113.0, 112.0, 110.9, 110.3, 102.3, 63.7. HRMS calcd for [C₃₂H₁₈N₂O₂⁺]: 462.1368, found: 462.1382.

Synthesis of 4c: Compound **4c** was prepared following the GP2 at 70 °C with **1c** (63.5 mg, 0.25 mmol), oAC-air(Δ) (113.5 mg) and MsOH (33.1 μ L, 0.51 mmol) with 16 h reaction time. Product was purified using flash column chromatography with silica as stationary phase and EtOAc:*n*-Hex (1:4) as eluent. Yield was 25.8 mg, 41%. ¹H NMR (500 MHz, [D₆]DMSO): δ = 12.45 (s, 1H), 8.40 (d, *J* = 8.0 Hz, 1H), 8.36 (d, *J* = 7.4 Hz, 1H), 8.17 (d, *J* = 8.2 Hz, 1H), 8.14 (d, *J* = 8.1 Hz, 1H), 7.83 (d, *J* = 7.7 Hz, 1H), 7.64 (d, *J* = 7.6 Hz, 1H), 7.59–7.52 (m, 4H), 7.49–7.44 (m, 2H), 7.28 (dd, *J* = 8.1, 7.0 Hz, 1H), 7.21 (dd, *J* = 8.1, 7.0 Hz, 1H), 7.19–7.12 (m, 2H), 6.67 (d, *J* = 0.7 Hz, 1H). ¹³C NMR (75 MHz, [D₆]DMSO): δ = 178.8, 155.9, 146.5, 139.5, 138.7, 138.5, 138.3, 137.8, 137.5, 135.6, 129.8, 129.4, 126.7, 126.1, 126.1, 125.7, 125.6, 124.3, 124.3, 124.1, 123.4 (3C), 123.3, 122.1, 121.7, 121.1, 120.0 (2C), 114.9, 112.6, 64.6. ¹H NMR (500 MHz, [D₆]acetone): δ = 11.36 (s, 1H), 8.52 (d, *J* = 7.9 Hz, 1H), 8.41 (d, *J* = 7.7 Hz, 1H), 8.26 (d, *J* = 8.1 Hz, 1H), 8.02 (d, *J* = 8.1 Hz, 1H), 7.85–7.80 (m, 1H), 7.61 (d, *J* = 7.6 Hz, 1H), 7.55 (dtd, *J* = 12.0, 7.9, 1.1 Hz, 3H), 7.51–7.42 (m, 3H), 7.28 (dd, *J* = 8.2, 7.0 Hz, 1H), 7.23 (dd, *J* = 8.2, 7.0 Hz, 1H), 7.18–7.12 (m, 2H), 6.74 (d, *J* = 0.8 Hz, 1H). ¹³C NMR (126 MHz, [D₆]acetone): δ = 180.1, 157.6, 148.0, 141.1, 140.2, 140.1, 139.8, 138.8, 138.6, 137.2, 131.2, 130.1, 127.4, 127.3, 127.1, 126.8, 126.4, 126.0, 125.0, 125.0, 124.8, 124.4, 124.1, 123.7, 122.8, 122.7, 122.1, 121.4, 121.3, 116.9, 113.4, 66.2. HRMS calcd for [C₃₂H₁₈S₂N₂⁺]: 494.0911; found: 494.0893 (Figure 7).

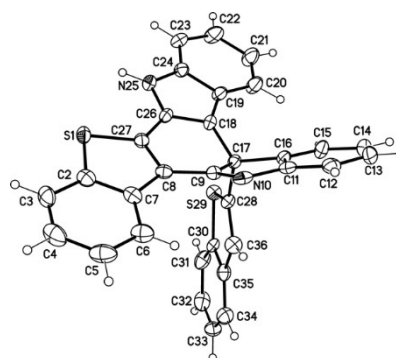


Figure 7. Molecular structure of one of the two crystallographic independent molecules of **4c** (see Supporting Information).

Acknowledgements

Financial support from Academy of Finland [project no. 129062 (J.H.)] is acknowledged. The Finnish National Centre for Scientific Computing (CSC) is recognized for computational resources. D.S.C. is grateful to Magnus Ehrnrooth and Toso-Montanari Foundations for funding, and M.Sc. Mikko Mäkelä for introduction into carbocatalysis and techniques to prepare our catalysts. We also thank Dr. Sami Heikkinen for assistance in NMR analysis.

Conflict of interest

The authors declare no conflict of interest.

Keywords: C–C coupling · cyclooctatetraene · density functional calculations · heterogeneous catalysis · oxidative dehydrogenative coupling

- [1] Selected reviews: a) D. R. Dreyer, C. W. Bielawski, *Chem. Sci.* **2011**, *2*, 1233; b) S. Navalon, A. Dhakshinamoorthy, M. Alvaro, H. Garcia, *Chem. Rev.* **2014**, *114*, 6179–6212; c) C. K. Chua, M. Pumera, *Chem. Eur. J.* **2015**, *21*, 12550–12562; d) D. S. Su, G. Wen, S. Wu, F. Peng, R. Schlögl, *Angew. Chem. Int. Ed.* **2017**, *56*, 936–964; *Angew. Chem.* **2017**, *129*, 956–985.
- [2] Examples of FC mechanism by GO catalysis: a) F. Hu, M. Patel, F. Luo, C. Flach, R. Mendelsohn, E. Garfunkel, H. He, M. Szostak, *J. Am. Chem. Soc.* **2015**, *137*, 14473–14480; b) H. Wu, C. Su, R. Tandiana, C. Liu, C. Qiu, Y. Bao, J. Wu, Y. Xu, J. Lu, D. Fan, K. P. Loh, *Angew. Chem. Int. Ed.* **2018**, *57*, 10848–10853; *Angew. Chem.* **2018**, *130*, 11014–11019; c) H. Wu, C. Qui, Z. Zhang, B. Zhang, S. Zhang, Y. Xu, H. Zhou, C. Su, K. P. Loh, *Adv. Synth. Catal.* **2020**, *362*, 789–794.
- [3] a) T. Wirtanen, M. K. Mäkelä, J. Sarfraz, P. Ihalainen, S. Hietala, M. Melchionna, J. Helaja, *Adv. Synth. Catal.* **2015**, *357*, 3718–3726; b) T. Wirtanen, S. Aikonen, M. Muuronen, M. Melchionna, M. Kemell, F. Davodi, T. Kallio, T. Hu, J. Helaja, *Chem. Eur. J.* **2019**, *25*, 12288–12293; c) J. E. Perea-Buceta, T. Wirtanen, O.-V. Laukkanen, M. K. Mäkelä, M. Nieger, M. Melchionna, N. Huittinen, J. A. Lopez-Sanchez, J. Helaja, *Angew. Chem. Int. Ed.* **2013**, *52*, 11835–11839; *Angew. Chem.* **2013**, *125*, 12051–12055.
- [4] K. Mouri, N. Morimoto, Y. Takeuchi, Y. Nishina, *Sci. Rep.* **2016**, *6*, 25824.
- [5] P. Rempala, J. Kroulík, B. T. King, *J. Org. Chem.* **2006**, *71*, 5067–5081.
- [6] L. Zhai, R. Shukla, S. H. Wadumethrige, W. Rathore, *J. Org. Chem.* **2010**, *75*, 4748–4760.
- [7] a) M. Grzybowski, K. Skonieczny, H. Butenschön, D. T. Gryko, *Angew. Chem. Int. Ed.* **2013**, *52*, 9900–9930; *Angew. Chem.* **2013**, *125*, 10084–10115; b) M. Grzybowski, B. Sadowski, H. Butenschön, D. T. Gryko, *Angew. Chem. Int. Ed.* **2020**, *59*, 2998–3027; *Angew. Chem.* **2020**, *132*, 3020–3050.
- [8] R. Willstätter, E. Waser, *Ber. Dtsch. Chem. Ges.* **1911**, *44*, 3423–3445.
- [9] W. Reppe, O. Schlichting, K. Klager, T. Toepel, *Justus Liebigs Ann. Chem.* **1948**, *560*, 1–92.
- [10] Selected transition metal mediated methods: a) a review: C. Wang, Z. Xi, *Chem. Commun.* **2007**, 5119; b) Pd-catalysis: K. Fukuzumi, Y. Nishii, M. Miura, *Angew. Chem. Int. Ed.* **2017**, *56*, 12746–12750; *Angew. Chem.* **2017**, *129*, 12920–12924.
- [11] COT reviews: a) A. Rajca, S. Rajca, M. Pink, M. Miyasaka, *Synlett* **2007**, 1799–1822; b) H. Huang, C.-K. Hau, C. C. M. Law, H. N. C. Wong, *Org. Biomol. Chem.* **2009**, *7*, 1249–1257; c) J.-W. Han, J.-X. Chen, X. Li, X.-S. Peng, H. N. C. Wong, *Synlett* **2013**, *24*, 2188–2198.
- [12] K. Xu, J. Huang, S. Lei, H. Su, F. Y. C. Boey, Q. Li, J. Yang, *J. Chem. Phys.* **2009**, *131*, 104704.
- [13] O. Talaz, N. Saracoglu, *Tetrahedron* **2010**, *66*, 1902–1910.
- [14] M. J. Marsella, R. J. Reid, *Macromolecules* **1999**, *32*, 5982–5984.
- [15] a) K. Fries, W. Pfaffendorf, *Ber. Dtsch. Chem. Ges.* **1911**, *44*, 114–123; b) J. Bergman, B. Egestad, *Tetrahedron Lett.* **1978**, *19*, 3143–3146.
- [16] a) H. Hiyoshi, T. Sonoda, S. Mataka, *Heterocycles* **2006**, *68*, 763–769; b) F. Wang, X.-C. Li, W.-Y. Lai, Y. Chen, W. Huang, F. Wudl, *Org. Lett.* **2014**, *16*, 2942–2945; c) L. Wang, Q. Fang, Q. Lu, S.-J. Zhang, Y.-Y. Jin, Z.-Q. Liu, *Org. Lett.* **2015**, *17*, 4164–4167.
- [17] K. Mouri, S. Saito, I. Hisaki, S. Yamaguchi, *Chem. Sci.* **2013**, *4*, 4465–4469.
- [18] A. Fukazawa, H. Oshima, S. Shimizu, N. Kobayashi, S. Yamaguchi, *J. Am. Chem. Soc.* **2014**, *136*, 8738–8745.
- [19] a) Q. Lin, Q. Li, C. Batchelor-McAuley, R. G. Compton, *J. Phys. Chem. C* **2015**, *119*, 1489–1495; b) E. Laviron, *J. Electroanal. Chem.* **1984**, *164*, 213–227.
- [20] A modified heat treatment procedure based on: J. L. Figueiredo, M. F. R. Pereira, M. M. A. Freitas, J. J. M. Órfão, *Carbon* **1999**, *37*, 1379–1389. Full characterization and discussion of oAC materials in: L. Enders, D. Casadio, S. Aikonen, A. Lenarda, T. Wirtanen, T. Hu, S. Hietala, L. S. Ribeiro M. F. R. Pereira, J. Helaja, *submitted*.
- [21] S. P. Roche, J.-J. Y. Tendoung, B. Tréguier, *Tetrahedron* **2015**, *71*, 3549–3591.
- [22] A. Vijay Kumar, K. R. Rao, *Tetrahedron Lett.* **2011**, *52*, 5188–5191.
- [23] T. Wirtanen, M. Muuronen, J. Hurmalainen, H. M. Tuononen, M. Nieger, J. Helaja, *Org. Chem. Front.* **2016**, *3*, 1738–1745.
- [24] S. Wu, G. Wen, X. Liu, B. Zhong, D. S. Su, *ChemCatChem* **2014**, *6*, 1558–1561.
- [25] Y.-M. Wang, Z. Wen, X.-M. Chen, D.-M. Du, T. Matsuura, J.-B. Meng, *J. Heterocycl. Chem.* **1998**, *35*, 313–316.
- [26] T. Niu, Y. Zhang, *Tetrahedron Lett.* **2010**, *51*, 6847–6851.
- [27] M. R. Accolla, M. Mauro, L. Falivene, L. Cavallo, G. Guerra, *ACS Catal.* **2014**, *4*, 492–496.
- [28] T. Nakayama, N. Okumura, B. Uno, *J. Phys. Chem. B* **2020**, *124*, 848–860.
- [29] a) G. A. Olah, J. S. Staral, G. Liang, L. A. Paquette, W. P. Melega, M. J. Carmody, *J. Am. Chem. Soc.* **1977**, *99*, 3349–3335; b) H. Hamaoka, S. Shiro-ma, K. Aburaya, M. Hasegawa, T. Nishinaga, *ChemPlusChem* **2019**, *84*, 704–711.
- [30] F. Furche, R. Ahlrichs, C. Hättig, W. Klopper, M. Sierka, F. Weigend, *WIREs Comput. Mol. Sci.* **2014**, *4*, 91–100.
- [31] F. Neese, *WIREs Comput. Mol. Sci.* **2017**, *8*, e1327.
- [32] P. Pracht, F. Bohle, S. Grimme, *Phys. Chem. Chem. Phys.* **2020**, *22*, 7169–7192.
- [33] a) S. Grimme, C. Bannwarth, P. Shushkov, *J. Comput. Theory Chem.* **2017**, *13*, 1989–2009; b) C. Bannwarth, S. Ehlert, S. Grimme, *J. Comput. Theory Chem.* **2019**, *15*, 1652–1671.
- [34] C. Adamo, V. Barone, *J. Chem. Phys.* **1999**, *110*, 6158–6170.
- [35] S. Grimme, S. Ehrlich, L. Goerigk, *J. Comput. Chem.* **2011**, *32*, 1456–1465.
- [36] F. Weigend, R. Ahlrichs, *Phys. Chem. Chem. Phys.* **2005**, *7*, 3297–3305.
- [37] Y. Zhao, D. G. Truhlar, *J. Phys. Chem. A* **2005**, *109*, 5656–5667.
- [38] D. Rappoport, F. Furche, *J. Chem. Phys.* **2010**, *133*, 134105.
- [39] a) M. Sierka, A. Hoge-kamp, R. Ahlrichs, *J. Chem. Phys.* **2003**, *118*, 9136–9148; b) K. Eichkorn, O. Treutler, H. Öhm, M. Häser, R. Ahlrichs, *Chem. Phys. Lett.* **1995**, *240*, 283–290.
- [40] F. Weigend, *Phys. Chem. Chem. Phys.* **2006**, *8*, 1057–1065.
- [41] A. Schäfer, A. Klamt, D. Sattel, J. C. W. Lohrenz, F. Eckert, *Phys. Chem. Chem. Phys.* **2000**, *2*, 2187–2193.
- [42] a) COSMOtherm, Version C3.0, Release 19.01; COSMOlogic GmbH & Co. KG, <http://www.cosmologic.de>; b) F. Eckert, A. Klamt, *AIChE J.* **2002**, *48*, 369; c) A. Klamt, V. Jonas, T. Bürger, J. C. Lohrenz, *J. Phys. Chem. A* **1998**, *102*, 5074; d) A. Klamt, *J. Phys. Chem.* **1995**, *99*, 2224.
- [43] a) A. D. Becke, *Phys. Rev. A* **1988**, *38*, 3098; b) J. P. Perdew, *Phys. Rev. B* **1986**, *33*, 8822.
- [44] A. Hellweg, F. Eckert, *AIChE J.* **2017**, *63*, 3944–3954.
- [45] S. Grimme, *Chem. Eur. J.* **2012**, *18*, 9955–9964. Authors also thank Prof. S. Grimme for providing the thermo-program for using the quasi-RRHO.
- [46] a) C. Hättig, A. Köhn, *J. Chem. Phys.* **2002**, *117*, 6939; b) C. Hättig, *Adv. Quant. Chem.* **2005**, *50*, 37–60.
- [47] R. Send, V. R. I. Kaila, D. Sundholm, *J. Chem. Phys.* **2011**, *134*, 214114.
- [48] a) R. Send, C.-M. Suomivuori, V. R. I. Kaila, D. Sundholm, *J. Phys. Chem. B* **2015**, *119*, 2933–2945; b) C.-M. Suomivuori, H. Fliegl, E. B. Starikov, T. S. Balaban, V. R. I. Kaila, D. Sundholm, *Phys. Chem. Chem. Phys.* **2019**, *21*, 6851–6858.
- [49] P. J. Stephens, N. Harada, *Chirality* **2010**, *22*, 229–333.
- [50] T. Bruhn, A. Schaumlöffel, Y. Hemberger, G. Bringmann, *Chirality* **2013**, *25*, 243–249.
- [51] J. Jusélius, D. Sundholm, J. Gauss, *J. Chem. Phys.* **2004**, *121*, 3952–3963.
- [52] S. Taubert, D. Sundholm, J. Jusélius, *J. Chem. Phys.* **2011**, *134*, 054123:1–12.
- [53] a) A. D. Becke, *J. Chem. Phys.* **1993**, *98*, 5648–5652; b) C. Lee, W. Yang, R. G. Parr, *Phys. Rev. B* **1988**, *37*, 785–789.
- [54] Gaussian 16, Revision C.01, M. J. Frisch, G. W. Trucks, H. B. Schlegel, G. E. Scuseria, M. A. Robb, J. R. Cheeseman, G. Scalmani, V. Barone, G. A. Petersson, H. Nakatsuji, X. Li, M. Caricato, A. V. Marenich, J. Bloino, B. G. Janesko, R. Gomperts, B. Mennucci, H. P. Hratchian, J. V. Ortiz, A. F. Izmaylov, J. L. Sonnenberg, D. Williams-Young, F. Ding, F. Lipparini, F. Egidi, J.

Goings, B. Peng, A. Petrone, T. Henderson, D. Ranasinghe, V. G. Zakrzewski, J. Gao, N. Rega, G. Zheng, W. Liang, M. Hada, M. Ehara, K. Toyota, R. Fukuda, J. Hasegawa, M. Ishida, T. Nakajima, Y. Honda, O. Kitao, H. Nakai, T. Vreven, K. Throssell, J. A. Montgomery, Jr., J. E. Peralta, F. Ogliaro, M. J. Bearpark, J. J. Heyd, E. N. Brothers, K. N. Kudin, V. N. Staroverov, T. A. Keith, R. Kobayashi, J. Normand, K. Raghavachari, A. P. Rendell, J. C. Burant, S. S. Iyengar, J. Tomasi, M. Cossi, J. M. Millam, M. Klene,

C. Adamo, R. Cammi, J. W. Ochterski, R. L. Martin, K. Morokuma, O. Farkas, J. B. Foresman, D. J. Fox, Gaussian, Inc., Wallingford CT, 2016.

Manuscript received: December 21, 2020

Accepted manuscript online: January 11, 2021

Version of record online: February 18, 2021
